

## Effect of polarization on photodetachment thresholds

J. Sandström,<sup>1</sup> G. Haefliger,<sup>1</sup> I. Kiyani,<sup>1,\*</sup> U. Berzinsh,<sup>1</sup> D. Hanstorp,<sup>1</sup> D. J. Pegg,<sup>2</sup> J. C. Hunnell,<sup>3</sup> and S. J. Ward<sup>3</sup><sup>1</sup>*Department of Physics, Chalmers University of Technology/Göteborg University, S-412 96 Göteborg, Sweden*<sup>2</sup>*Department of Physics, University of Tennessee, Knoxville, Tennessee 37996, USA*<sup>3</sup>*Department of Physics, University of North Texas, Denton, Texas 76203, USA*

(Received 3 December 2003; revised manuscript received 22 June 2004; published 16 November 2004)

We have measured the near-threshold cross sections for the photodetachment of  $\text{Li}^-$  into the  $e^-(ks, d)\text{-Li}(2p_{1/2})$ ,  $e^-(ks, d)\text{-Li}(3p)$ ,  $e^-(kp)\text{-Li}(3s)$ , and  $e^-(kp)\text{-Li}(4s)$  continuum channels and the photodetachment of  $\text{K}^-$  into the  $e^-(ks, d)\text{-K}(4p_{3/2})$  continuum channel. The data was analyzed using both a top-of-barrier model and a modified effective range theory. Both approaches explicitly take into account the significant polarization potential in the final continuum channels. The study involving both experiment and theory enabled us to investigate the effect of the polarization on near-threshold photodetachment. Furthermore, since photodetachment and electron scattering are related in the half-collision concept, we were able to determine low-energy electron scattering quantities such as phase shifts, elastic cross sections, and  $s$  wave scattering lengths for electron scattering on excited Li and K atoms. The results allowed us to predict a virtual state in the  $e^-(ks)\text{-Li}(3p)$  system.

DOI: 10.1103/PhysRevA.70.052707

PACS number(s): 32.80.Gc, 34.80.Bm

## I. INTRODUCTION

In this paper we explore, in a systematic manner, the effect of the polarization on cross sections for photodetachment in the vicinity of excited-state thresholds. We consider specifically the photodetachment of  $\text{Li}^-$  and  $\text{K}^-$ . The dipole polarizabilities of excited states of the alkali-metal atoms are large.

In a one-photon detachment process a single electron is detached from a negative ion following the absorption of a single photon. This bound-free transition can be represented as

$$h\nu + X^-(i) \rightarrow X(f) + e^-(k\ell). \quad (1)$$

The final continuum state channel in the above reaction is characterized by the quantum state of the residual atom and the linear ( $k$ ) and angular ( $\ell$ ) momenta of the detached electron. In the present work the residual atom is left in an excited state following detachment. The threshold behavior of the cross section for photodetachment process is determined by the interaction between the residual atom and the electron. Just above the threshold for the opening of this continuum channel, the energy dependence of the cross section for photodetachment from an atomic negative ion is governed by the Wigner law [1]

$$\sigma = Ak^{2\ell+1} = B(E - E_{th})^{\ell+1/2}, \quad (2)$$

where  $E = \hbar\omega$  is the photon energy,  $E_{th}$  is the threshold energy and  $\ell$  represents the lowest allowed orbital angular momentum of the detached electron. Higher values of the angular momentum are effectively suppressed by the presence of the centrifugal barrier.

The Wigner law has been successfully tested for both  $s$  and  $p$  wave detachment [2–4]. However, the energy range of validity of the Wigner law is limited if the dipole polarizability of the residual atom in the final continuum state is large, as it is in the case of excited states. The first photodetachment experiments on threshold behavior for leaving alkali atoms in excited state were conducted more than 20 years ago [5–8]. Theory does not predict the range of validity of the Wigner law. In the derivation of the Wigner law it is assumed that the interaction between the ejected electron and the residual atom fall off faster than  $1/r^2$  at large distances. In reality, however, the electron induces an electric dipole moment in the atom, which is proportional to the dipole polarizability of the atom. The induced dipole thus formed acts back on the electron. The interaction between the ejected electron and the electric dipole is the polarization potential,  $-\alpha/2r^4$ , where  $\alpha$  is the dipole polarizability of the state of the atom. The effect of the polarization potential on the near-threshold behavior of the photodetachment cross section will be most significant when the residual atom has a large polarizability. O'Malley *et al.* [9] developed a modified effective range theory (MERT) applicable to the polarization potential. The exact solutions to the Schrödinger equation with the polarization potential are  $r^{1/2}M_{\pm\tau}[\ln(k/f)^{1/2}r]$ , where  $M_{\pm\tau}$  are Mathieu functions of order  $\pm\tau$ ,  $\tau$  is the characteristic exponent and  $f = \sqrt{\alpha}$  [10–12]. In the derivation of the MERT of O'Malley *et al.* [9],  $\tau$  and the ratio  $m = M_{+\tau}(0)/M_{-\tau}$  are expanded in terms of  $fk$ . Because of this, the range of applicability of the MERT of O'Malley *et al.* is very small when  $\alpha$  is large. Watanabe and Greene [11] and Fabrikant [13] developed MERTs for the polarization potential in which they retained the exact values of  $\tau$  and  $m$ . These MERTs can, therefore, be applied over a wider energy range than the MERT of O'Malley *et al.*

We have applied the single-channel version of the MERT of Watanabe and Greene (WGMERT) to fit measured cross sections for the photodetachment of  $\text{Li}^-$  into the  $e^-(ks, d)$

\*Present address: Physics Department, Freiburg University, Hermann-Herder-Str. 3, D-79104 Freiburg, Germany.

$-Li(2p_{1/2})$ ,  $e^-(ks,d)-Li(3p)$ ,  $e^-(kp)-Li(3s)$ , and  $e^-(kp)-Li(4s)$  final-state channels, and for the photodetachment of  $K^-$  into the  $e^-(ks,d)-K(4p_{3/2})$  channel. With the WGMERT, the data can be fitted over a much broader energy range than it could be with either the Wigner law or the MERT of O'Malley *et al.* We used the MERT of Fabrikant (FMERT) [13] to obtain virtual state energies of the  $e^-(ks)-Li(2p_{1/2})$ ,  $e^-(ks)-Li(3p)$  and  $e^-(ks)-K(4p_{3/2})$  systems. We also fitted the photodetachment data using a top-of-barrier (TOB) model [14]. In the analysis we neglected the quadrupole interaction between a residual atom in a  $np_{3/2}$  state and an outgoing  $d$  wave electron. This should be a reasonable approximation since the  $d$  wave contribution to the near-threshold photodetachment cross section should be small compared to the  $s$  wave contribution due to the centrifugal barrier. Our analysis of the cross section for the photodetachment of  $Li^-$  into the final-state channel of  $e^-(ks,d)-Li(2p_{1/2})$  has been reported elsewhere [15].

Previously, Moores and Norcross [16] computed the photodetachment cross sections for  $Li^-$ ,  $Na^-$  and  $K^-$  using for the final state close-coupling wave functions that were obtained using the LS representation. They noted that the range of validity of the Wigner law is very narrow for the cross section of the photodetachment of the alkali negative ion into an electron and the first excited state of the alkali atom above the threshold of that excited state. Taylor and Norcross [17] computed the cross section for the photodetachment of  $K^-$  into  $e^-(ks)$  and  $K(4p_{3/2})$  continuum channel in the vicinity of the  $K(4p_{3/2})$  threshold. They performed a four-state close-coupling calculation of the  $e^-K$  collision process in which they retained the  $4s^2S^e$ ,  $4p^2P^o$ ,  $3d^2D^e$ , and  $5s^2S^e$  states of the atom. The equations were formulated in the LS representation. The matrix elements computed were fitted to a quadratic form representation, and the fits were used to compute the photodetachment cross section in the  $jj$  coupling scheme.

Photodetachment involving an excited residual atom in the final continuum state, is equivalent, in the half-collision concept, to electron scattering on an excited atomic target. The latter process has received little attention experimentally due to the technical difficulties associated with target preparation and the production of low-energy electrons. In the present work we have been able to circumvent this problem by extracting information on low-energy electron-excited atom scattering from WGMERT fits to the corresponding measured photodetachment threshold data. Parameters derived from these fits have been used to investigate the effect of a highly polarizable atom target on the scattering of low-energy electrons. Polarization-sensitive quantities such as phase shifts,  $s$  wave scattering lengths, virtual states and Ramsauer minima have been obtained from the fits to the measured data.

## II. EXPERIMENTAL PROCEDURE

We investigated the threshold behavior of partial photodetachment cross sections of the type

$$h\nu + X^-(^1S) \rightarrow X^*(np) + e^-(ks,d). \quad (3)$$

The residual atom is left in a  $np$  excited state following detachment and the detached electron is described by  $s$  and  $d$

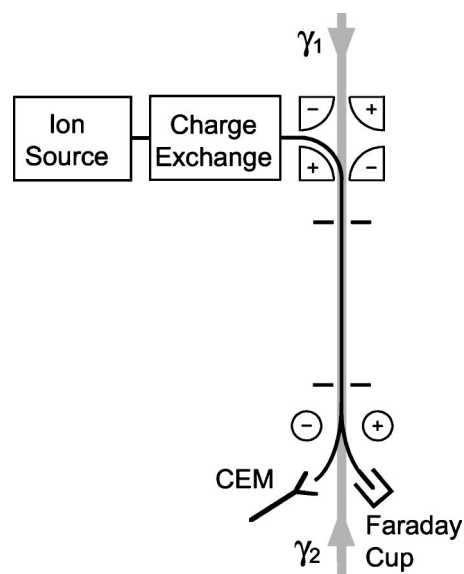


FIG. 1. Schematic of the collinear laser-ion beam apparatus used in the photodetachment experiments. A beam of negative ions is merged with two laser beams labeled  $\gamma_1$  and  $\gamma_2$ . Atoms are created in the interaction region as a result of detachment induced by the  $\gamma_1$  laser. These atoms, after being excited to Rydberg states by the  $\gamma_2$  laser, are stripped in an electric field generated by the vertical electrodes labeled + and -. Positive ions, produced in this state-selective detection scheme, are detected using a channel electron multiplier (CEM).

waves. The electron detachment plus excitation processes were studied for three cases in which the excited residual atoms were left in the  $Li(2p_{1/2})$ ,  $Li(3p)$ , and  $K(4p_{3/2})$  states. We also measured near-threshold partial cross sections for processes of the type

$$h\nu + X^-(^1S) \rightarrow X^*(ns) + e^-(kp), \quad (4)$$

where the outgoing electron is described by a  $p$  wave. Here, the excited residual atoms were left in the  $Li(3s)$  and  $Li(4s)$  states. In the case of the photodetachment of  $K^-$ , we were able to resolve the fine structure splitting between  $K(4p_{1/2})-K(4p_{3/2})$ . Similarly, we were also able to resolve the fine structure splitting between  $Li(2p_{1/2})$  and  $Li(2p_{3/2})$ . We measured the partial cross section for the photodetachment of  $K^-$  into the  $e^-K(4p_{3/2})$  continuum above the  $K(4p_{3/2})$  threshold. We also measured the partial cross section for the photodetachment of  $Li^-$  into the  $e^-Li(2p_{1/2})$  continuum above the  $Li(2p_{1/2})$  threshold. In the case of the photodetachment of  $Li^-$  into the  $e^-Li(3p)$  continuum the extremely small fine structure between  $Li(3p_{1/2})$  and  $Li(3p_{3/2})$  splitting was not resolved.

In the photodetachment measurements, two laser beams and a negative ion beam were merged collinearly. A schematic of the apparatus is shown in Fig. 1. Details of the experimental procedures can be found in two earlier papers by Haefliger *et al.* [18] and Andersson *et al.* [19]. The advantage of the collinear beam geometry is that it allows one to simultaneously enhance both the sensitivity and energy resolution of the measurement. The high sensitivity was achieved

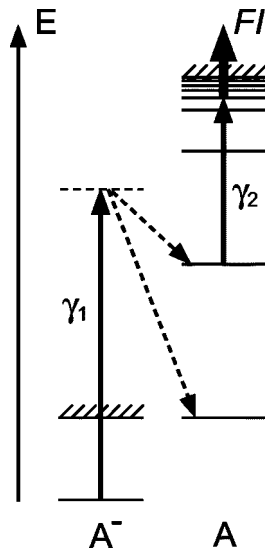


FIG. 2. A typical two-color laser scheme used to detach electrons from negative ions and to state-selectively detect the residual atoms produced in the process. The arrow labeled FI represents the electric field ionization process.

by using an interaction volume that was 0.7 m long and by efficiently collecting and selectively detecting the residual atoms produced in the detachment process. The high energy resolution is the result of the significant reduction in kinematic broadening that is inherent in the collinear arrangement. The longitudinal velocity distribution associated with the ions leaving the ion source is compressed upon acceleration. This phenomenon, however, can only be exploited in the collinear beam geometry. In the present apparatus the energy resolution, which was approximately  $25 \mu\text{eV}$ , was determined solely by the bandwidth of the laser. The beam of negative ions was extracted from an ion source, accelerated to the desired energy, which was typically a few keV, and then mass analyzed. The interaction region was carefully shielded in order to avoid stray electric fields from the field ionizer to leak into the interaction region. An electrostatic quadrupole deflector was used to merge the ion beam with the laser beams.

A typically two-color selective detection scheme is shown in Fig. 2. One laser was used to detach electrons from the moving ions in the beam. The wavelength of this laser was scanned in each experiment in the vicinity of the threshold for the opening of the particular partial detachment channel of interest. In the case of the  $\text{Li}(2p_{1/2})$  and  $\text{K}(4p_{3/2})$  thresholds, this laser was operated in the visible. In the case of the  $\text{Li}(3s)$ ,  $\text{Li}(3p)$  and  $\text{Li}(4s)$  thresholds, the laser was operated in the ultraviolet wavelength region. An excimer-pumped dye laser was used to generate the visible radiation and the visible output of the dye laser was frequency doubled to generate the ultraviolet radiation. Both the fundamental and frequency-doubled laser light were linearly polarized. The wavelength scale of the dye laser was calibrated using well-known reference lines generated by optogalvanic spectroscopy when a portion of the laser beam is passed through a hollow cathode lamp filled with Ar or Ne. These reference lines were used to establish an absolute scale. A fraction of

the laser beam was also passed through a calibrated Fabry-Pérot interferometer in order to generate fringes that were used to interpolate between the absolute wavelength markers. A second laser was used in the state-selective detection process. This laser was operated in the visible. Since more than one photodetachment channel is open at an excited state threshold, one must isolate the particular continuum channel of interest in order to study the corresponding partial cross section. State-selective detection of the  $\text{Li}(2p_{1/2})$ ,  $\text{Li}(3s)$ ,  $\text{Li}(3p)$ , and  $\text{K}(4p_{3/2})$  atoms was achieved by using the second laser to resonantly photoexcite these residual atoms to a high-lying Rydberg state before they had time to relax radiatively. The Rydberg atoms so produced were efficiently ionized by applying an electric field to the beam. The resonant ionization process, however, was not applicable to the selective detection of  $\text{Li}(4s)$  atoms since the  $4s$  state lies too close to the ionization limit for visible radiation to be used in the resonant step, and tunable infrared sources were unavailable to us at the time of the experiment. In this case, the residual  $\text{Li}(4s)$  atoms were directly photoionized. To partially compensate for the smaller cross section associated with the non-resonant step, we used a more powerful laser, a Nd:YAG laser. The yields of positive ions produced in either the resonant or non-resonant ionization processes were normalized to the intensity of the first laser and the ion beam current. This normalized signal, which is proportional to the partial cross section, was used to monitor the behavior of the cross section near threshold. The signal-to-background ratio for the detection of positive ions was high since background contributions from positive ions arising from double detachment in collisions with gas particles were small at the residual pressure of  $10^{-9}$  mbar typically used in the experiments. This background contribution was measured when the pulsed laser was off. The collisional detachment background was further reduced by using time-resolved detection. The timing cycle was initiated by the laser pulse. The detection of the positive ions, arising from the resonance ionization of the residual atoms, was delayed relative to the laser pulse to account for the finite time of flight between the interaction region and the detector. A narrow time window was set up in the electronics to coincide with the arrival of the positive ions at the detector. Within this time window the contribution from the collisionally-induced background is small since these events are randomly distributed in time. The experimental data was corrected for the Doppler shift. This could be performed since the velocity of the accelerated ions is well known. A Wigner law fit, Eq. (2), was then applied to the data in order to determine the experimental threshold position. Generally, the Wigner law is considered valid if the deviation of the fit representing the law in some energy range is less than some arbitrarily chosen fraction. The range of validity of the Wigner law was determined based on a 10% criterion. The data was fit to a nonlinear least squares function and the threshold energies were determined from the best fit to the data. The uncertainty in the threshold energies which are given in Sec. IV represent the quadrature summation of several uncertainties. These uncertainties are the uncertainty from the calibration of the laser wavelength, the uncertainty in the velocity of the ions and the uncertainty in the fit to the Wigner law. In the case of thresholds where the

TABLE I. Static dipole polarizabilities,  $\alpha$  [11,21].

Excited-state atom	$\alpha$
Li(2 <i>p</i> )	126.8
Li(3 <i>p</i> )	28235
Li(3 <i>s</i> )	4130.5
Li(4 <i>s</i> )	35233.5
K(4 <i>p</i> )	600

residual atom is left in an excited *s* state, the uncertainty from the calibration of the laser wavelength is the dominating term in determining the uncertainty in the threshold energy. For the thresholds where the residual atom is left in an excited *p* state, the uncertainty in the fit to the Wigner law gives the largest contribution.

### III. THEORY

To adequately describe the near-threshold photodetachment of alkali-metal negative ions into a free electron and an excited state alkali-metal atom, the polarization potential in the final continuum channel needs to be explicitly taken into account. This we did by applying the single-channel version of WGMERT [11], FMERT [13], and the TOB model [14]. The appropriate polarizability to use is the channel polarizability  $\alpha_{n\ell_1 k\ell}$ , where *n* and  $\ell_1$  are respectively the principal quantum number and orbital angular momentum of the residual atom [11]. The channel polarizability reduces to the static dipole polarizability for all the channels we considered except for the channels where the residual atom is in a *p* state and the ejected electron is a *d* wave [20]. However, the *d* wave contribution to the photodetachment cross section near threshold should be small due to the centrifugal barrier. In our analysis we used the static dipole polarizability for all the channels we considered. We quote the values of the static dipole polarizability in Table I. The static dipole polarizabilities of the excited states of Li were computed by Sadeghpour [21]. The static dipole polarizability for K(4*p*) was obtained from Ref. [11]. To check the approximation of using the static dipole polarizability rather than the channel polarizability for the *npkd* channel, we also analyzed the  $K^-$  data using the channel polarizability ( $\alpha_{4pkd}=690$ ) for this channel [11]. We found that using the channel polarizability for the *npkd* channel rather than the static dipole polarizability changes the  $K^-$  total photodetachment cross section by less than 0.03%. In our analysis, we did not explicitly take into account spin-orbit coupling other than using the threshold energy of Li(2*p*<sub>1/2</sub>) and K(4*p*<sub>3/2</sub>). Throughout this paper we used atomic units unless explicitly stated.

The solutions to the Schrödinger equation for a charged particle and an atom interacting via the long-range polarization potential,  $-\alpha/2r^4$ , are  $r^{1/2}M_{\pm\tau}[\ln(k/f)^{1/2}r]$ , where  $M_{\pm\tau}$  are the Mathieu functions of order  $\pm\tau$  and  $f=\sqrt{\alpha}$  [10,11]. In transforming the Schrödinger equation to Mathieu's differential equation, the Langer factor  $(\ell+1/2)^2-\ell(\ell+1)=1/4$  is introduced, where  $\ell$  is the orbital angular momentum of the charged particle [12,14]. Thus, the long-range form of the

potential for scattering of a charged particle from an atom with a large polarizability is effectively the sum of a repulsive centrifugal-type potential and an attractive polarization potential,

$$V(r) = \frac{(\ell+1/2)^2}{2r^2} - \frac{\alpha}{2r^4}. \quad (5)$$

This potential gives rise to a barrier even for zero angular momentum.

Ward and Macek [14] derived an analytical expression for the transmission modulus squared term  $|T|^2$  describing tunneling through, and transmission over, the barrier that arises from the potential of Eq. (5). This expression is

$$|T|^2 = \frac{1}{1 + \exp(2\pi a)}, \quad (6)$$

where

$$a = \frac{\ell+1/2}{2} \frac{1-b}{\sqrt{1+b}} {}_2F_1\left(\frac{1}{2}, \frac{3}{2}; 2; \frac{1-b}{1+b}\right), \quad (7)$$

$$b = \frac{2\sqrt{\alpha k}}{(\ell+1/2)^2}, \quad (8)$$

and  ${}_2F_1(\frac{1}{2}, \frac{3}{2}; 2; (1-b)/(1+b))$  is a hypergeometric function. The quantity *k* is the linear momentum of the ejected electron. Expanding  $|T|^2$  about the threshold energy for excitation of the atom gives

$$|T|^2 \approx e^{-2\pi a} \approx \left(\frac{2\sqrt{\alpha k}}{8(\ell+1/2)^2}\right)^{2\ell+1}, \quad (9)$$

which has the same *k*-dependence as the Wigner law.

The height of the barrier is  $V_{\max}=(\ell+1/2)^4/8\alpha$ . Using this equation, the heights of the barriers for the  $e^-$ -Li(2*p*),  $e^-$ -Li(3*p*),  $e^-$ -Li(3*s*),  $e^-$ -Li(4*s*), and  $e^-$ -K(4*p*) continuum states are determined to be  $6.16 \times 10^{-5}$ ,  $2.7 \times 10^{-6}$ ,  $1.53 \times 10^{-4}$ ,  $1.8 \times 10^{-5}$  and  $1.3 \times 10^{-5}$ , respectively. For a given  $\ell$ , the height of the barrier is smaller the larger the polarizability. A low potential barrier results in a sharp increase of the photodetachment cross section, which is most pronounced in the case of an *s* wave ejected electron.

The TOB factor,  $|T|^2$ , describes the general behavior of the cross section for near-threshold photodetachment. However, a more detailed description of the cross section can be obtained using WGMERT [11]. This effective range theory explicitly takes into account the polarization potential. It was developed specifically for the problem of photodetachment of  $K^-$  in the energy range near the K(4*p*) detachment threshold, where  $e^-(ks)$ -K(4*p*) and  $e^-(kp)$ -K(4*s*) are open channels. Recently, Ward and Macek [14] and Ward *et al.* [15] used WGMERT to analyze *ab initio* calculations of  $e^+$ -H and  $e^+$ -He collisions, respectively. The analysis demonstrated that to describe the behavior of the near-threshold positronium formation cross section it is necessary to take into account explicitly the polarization potential in the effective range theory [14,15].

In the present work we applied WGMERT to the problem of the photodetachment of  $Li^-$  and  $K^-$  into continuum states

involving an electron and an excited-state atom. A comparison of the near-threshold cross section calculated using WGMERT with experimental photodetachment data enabled us to extract parameters that vary slowly with energy. From these slowly-varying parameters, one can obtain quantities associated with low-energy electron scattering from excited-state atoms. In applying WGMERT, we considered for each partial photodetachment cross section only the specific final-state continuum channel that was measured in the experiment. We did not take into account any other channel, whether open or closed. This enabled us to treat the problem as a single-channel problem and accordingly, we used the single-channel version of WGMERT. The advantage of treating the problem as a single-channel problem is that it enabled us to determine  $s$  wave scattering lengths, phase shifts and elastic cross sections for low-energy electron scattering from excited-state atoms.

Details of the derivation of WGMERT and its application to  $K^-$  photodetachment are given in Ref. [11]. In the Appendix we present the single-channel version of WGMERT that we used in the analysis of the experimental data. We give the WGMERT expression for the photodetachment cross section. We also compare the WGMERT equation for  $\tan \delta_\ell$  with a MERT for  $\tan \delta_\ell$ , Eq. (4.3) of O'Malley *et al.* [9], and state how the familiar O'Malley *et al.* MERT for  $k \cot \delta_\ell$  and  $\tan \delta_\ell$  ( $\ell \geq 1$ ) are obtained from this MERT. Furthermore, we compare the WGMERT equation for  $\tan \delta_\ell$  to the FMERT equation for  $\tan \delta_\ell$ .

The WGMERT expression for the partial wave photodetachment cross section for single channel scattering is given by Eq. (A16) from the Appendix

$$\sigma_{ph}^\ell = \frac{N'(\ell)\omega k^{2\ell+1}}{[\Gamma_{ff}(\ell) - K_{22}^{P0}(\ell)\Gamma_{gf}(\ell)]^2}. \quad (10)$$

The cross section is expressed in terms of quantities that vary slowly with energy,  $K_{22}^{P0}(\ell)$  and  $N'(\ell)$ , and quantities that vary rapidly with energy,  $\Gamma_{ff}(\ell)$  and  $\Gamma_{gf}(\ell)$ . The term  $N'(\ell) = N|D^{P0}(\ell)|^2$ , where  $N$  is the normalization constant of the partial wave photodetachment cross section [Eq. (A1)] and  $D^{P0}(\ell)$  is the part of the dipole matrix element that varies slowly with energy. In our analysis, we took  $K_{22}^{P0}(\ell)$  and  $D^{P0}(\ell)$  to be constants.

In the case of the photodetachment of the  $Li^-$  ion into a continuum state involving an excited  $Li(ns)$  atom, the ejected electron is described by a pure  $p$  wave. We extracted the slowly-varying parameters  $K_{22}^{P0}(\ell=1)$  and  $N'(\ell=1)$  by fitting the experimental relative cross section data to the WGMERT expression for the photodetachment cross section  $\sigma_{ph}^{\ell=1}$  at two points near threshold. Once  $K_{22}^{P0}(\ell=1)$  and  $N'(\ell=1)$  are determined we used them at all the other energies to compute the  $p$  wave photodetachment cross section  $\sigma_{ph}^{\ell=1}$ .

For the photodetachment of the  $Li^-$  and  $K^-$  ions into a continuum state involving a residual atom in an excited  $p$  state, the ejected electron is, in general, represented by both  $s$  and  $d$  waves. However, near threshold the  $s$  wave dominates over the  $d$  wave due to the centrifugal barrier associated with the latter. Therefore, we assumed that near threshold the ejected electron was entirely represented by a  $s$  wave.

The experimental data was fitted to the WGMERT expression for the  $s$  wave photodetachment cross section  $\sigma_{ph}^{\ell=0}$  at two points near threshold in order to extract  $N'(\ell=0)$  and  $K_{22}^{P0}(\ell=0)$ . It is known that the  $d$  wave contribution  $\sigma_{ph}^{\ell=2}$  to the photodetachment cross section becomes more significant as the energy above threshold is increased. We assumed that any difference between the  $s$  wave WGMERT fit and the experimental data at higher energies is due to the  $d$  wave contribution to the photodetachment cross section. With this assumption, we extracted  $K_{22}^{P0}(\ell=2)$  and  $N'(\ell=2)$  by fitting the WGMERT  $d$  wave photodetachment cross section to the difference between the experimental data and the WGMERT  $s$  wave photodetachment cross section. However, we recognize that a difference between the experimental data and the WGMERT  $s$  wave photodetachment cross section could also be due to the parameters  $K_{22}^{P0}(\ell=0)$  and  $N'(\ell=0)$  varying with energy or to multipole terms of higher order than the polarization potential. The partial cross section for the photodetachment of  $Li^-$  or  $K^-$  ions into an electron and an excited  $p$  atom is the sum of the  $s$  and  $d$  wave contributions.

Once the slowly varying parameter  $K_{22}^{P0}(\ell)$  has been defined, the  $\ell$  phase shifts ( $\delta_\ell$ ) associated with elastic scattering of an electron from a particular excited state of the atom can be determined from  $K_{22}^{P0}(\ell)$  according to Eq. (A17) from the Appendix

$$K_\ell = \tan \delta_\ell = k^{2\ell+1} \left( \frac{K_{22}^{P0}(\ell)\Gamma_{gg}(\ell) - \Gamma_{fg}(\ell)}{\Gamma_{ff}(\ell) - K_{22}^{P0}(\ell)\Gamma_{gf}(\ell)} \right), \quad (11)$$

where  $K_\ell$  is the single-channel  $K$ -matrix. The elements of the matrix  $\Gamma(\ell)$  are given in the Appendix. This is the WGMERT equation for  $\tan \delta_\ell$ . The corresponding elastic cross section is determined from the phase shift  $\delta_\ell$ .

Poles in the single-channel  $S$ -matrix are obtained by solving the equation,  $\tan \delta_\ell = -i$ . In solving this equation we used the form of the  $\tan \delta_\ell$  given by FMERT (see Appendix) and took the slowly varying parameter  $M$  to be a constant.

#### IV. RESULTS

Figures 3–6 show, respectively, the near-threshold cross sections for the photodetachment of  $Li^-$  into  $e^-(ks, d)$ - $Li(2p_{1/2})$ ,  $e^-(ks, d)$ - $Li(3p)$ ,  $e^-(kp)$ - $Li(3s)$ , and  $e^-(kp)$ - $Li(4s)$  continuum states. Figure 7 shows the cross section for the photodetachment of  $K^-$  into the  $e^-(ks, d)$ - $K(4p_{3/2})$  continuum. Also shown in Figs. 3–7 are the TOB and WGMERT fits to the experimental data. The nonstatistical fluctuations that appear in the experimental data are due to interference caused by multiple reflections in the optical components used in the experimental apparatus. In Table II we list the threshold energies that have been experimentally determined by fitting the Wigner law to the photodetachment signal in the near vicinity in each of the individual thresholds. In Table III we give the extracted slowly-varying parameter  $K_{22}^{P0}(\ell)$  for the  $e^-(ks)$ - $Li(2p_{1/2})$ ,  $e^-(ks)$ - $Li(3p)$ ,  $e^-(kp)$ - $Li(3s)$ ,  $e^-(kp)$ - $Li(4s)$  and  $e^-(ks)$ - $K(4p_{3/2})$  final continuum states. We also present in Table III the  $s$  wave scattering lengths  $A_0$  and the position of the poles  $k_p$  in the single-channel  $S$ -matrix obtained using  $K_{22}^{P0}(\ell)$ . Furthermore,

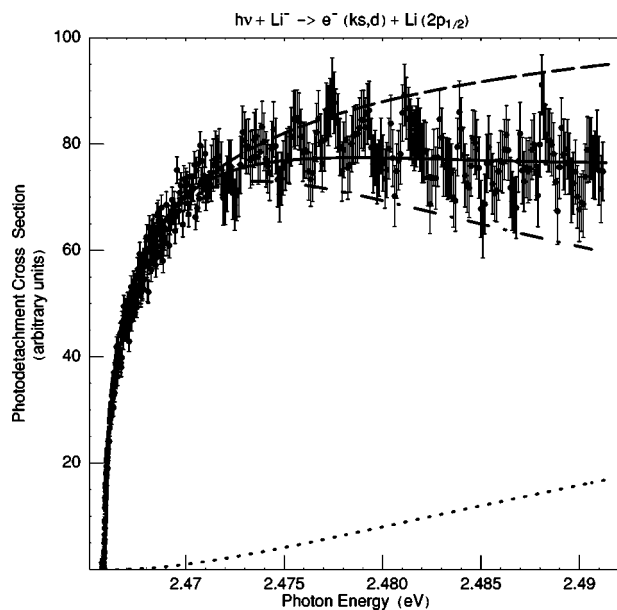


FIG. 3. The relative partial cross section for the photodetachment of  $\text{Li}^-$  into the  $e^-(ks,d)\text{-Li}(2p_{1/2})$  continuum above the  $\text{Li}(2p_{1/2})$  threshold. The experimental data is shown by the black solid circles, the sum of the  $s$  wave and extracted  $d$  wave WGMERT fits by the solid line, the  $s$  wave WGMERT fit by the dashed-dotted line, the extracted  $d$  wave WGMERT fit by the dotted line, and the TOB factor,  $|T|^2$ , normalized to the experimental data, is shown by the dashed line. The nonstatistical fluctuation with a frequency of about 0.002 eV is an artifact caused by multiple reflections in optical components that gives small fluctuations in the laser intensity.

in this table we give the uncertainties in  $K_{22}^{P0}(\ell)$ ,  $A_0$  and  $k_p$  that correspond to the uncertainty in the threshold energy.

The cross section for photodetachment of  $\text{Li}^-$  into the  $e^-(ks,d)\text{-Li}(2p_{1/2})$  continuum exhibits a steep rise above threshold over a very narrow energy range of only 3 meV (see Fig. 3). Beyond this, it changes much more slowly with energy. The cross section satisfies the Wigner law, but only over an extremely narrow energy range of 0.4 meV. The energy range over which the cross section sharply increases is approximately 50 times the height of the  $s$  wave barrier associated with the long-range potential given in Eq. (5). Both the TOB factor,  $|T|^2$ , and the  $s$  wave WGMERT cross section agree very well with the experimental data near threshold, and reasonably well over the entire energy range considered. The TOB factor,  $|T|^2$ , was normalized to the measured relative cross section data near the peak of the cross section, at a photon energy of  $E=2.46995$  eV. The  $s$  wave WGMERT cross section was fitted to two experimental data points near threshold, at  $E=2.4665$  eV and 2.4691 eV. This cross section falls below the experimental data after the peak in the cross section. We assumed that this difference is due to the neglect of the  $d$  wave WGMERT cross section. Using this assumption, we fitted the  $d$  wave WGMERT cross section to this difference at two energies above the threshold, at  $E=2.47962$  eV and 2.48689 eV. The sum of the  $s$  wave and the extracted  $d$  wave WGMERT cross sections agrees very well with the experimental data. From  $K_{22}^{P0}(\ell=0)$  that was

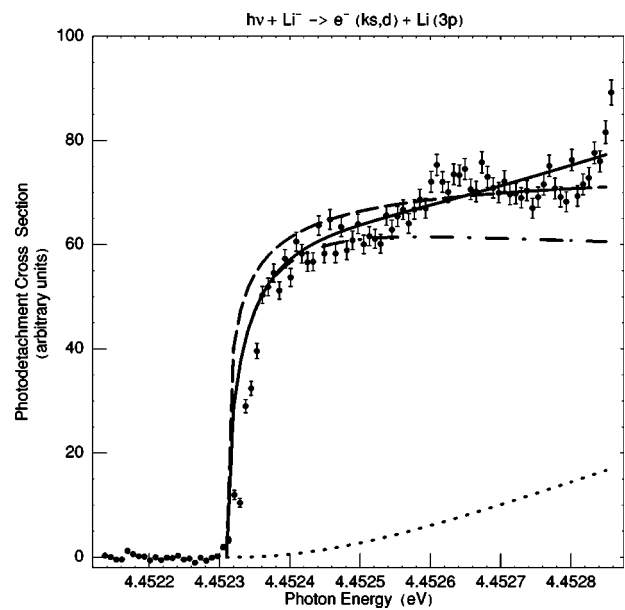


FIG. 4. The relative partial cross section for the photodetachment of  $\text{Li}^-$  into the  $e^-(ks,d)\text{-Li}(3p)$  continuum above the  $\text{Li}(3p)$  threshold. The experimental data is shown by the black solid circles, the sum of the  $s$  wave and extracted  $d$  wave WGMERT fits by the solid line, the  $s$  wave WGMERT fit by the dashed-dotted line, the extracted  $d$  wave WGMERT fit by the dotted line, and the TOB factor,  $|T|^2$ , normalized to the experimental data, is shown by the dashed line. The nonstatistical fluctuation, such as the small increase in the signal around 4.45265 eV, is an artifact caused by multiple reflections in optical components that causes small fluctuations in the laser intensity.

extracted from the fit, we determined quantities for low-energy  $e^-\text{-Li}(2p_{1/2})$  scattering. The  $s$  wave scattering length for  $e^-\text{-Li}(2p_{1/2})$  scattering is  $-65$ . This large and negative scattering length is indicative of a virtual state in the  $e^-(ks)\text{-Li}(2p_{1/2})$  system. The pole in the single channel  $S$ -matrix associated with the virtual state was found at  $k_p = -0.0008 - i0.01$ , corresponding to a virtual state energy of  $E_{vir} = -0.002 + i0.0003$  eV. Ward and Macek [14] reported that a virtual state pole for a polarization potential is slightly shifted to the left of the negative imaginary  $k$ -axis relative to its position for a short-range interaction. Only in the limit where the polarizability tends to zero is the pole on the negative imaginary axis at  $k_p = i/A_0$ .

Bae and Peterson [22] predicted a virtual state in the  $e^-(ks)\text{-Li}(2p)$  system at an energy 0.002 below the  $\text{Li}(2p)$  threshold. This energy corresponds to  $k_p = -i0.06$ . These investigators determined the value by applying Nesbet's multichannel scattering theory [23] to obtain a parametric form for the photodetachment cross section. However, the parametric form is strictly applicable to short-range interactions only. For short-range interactions, the scattering length  $A_0$  is given by  $A_0 = i/k_p$ . Bae and Peterson's value for the virtual state energy corresponds to a scattering length of  $-15.7$  [24]. These values of the scattering length and virtual-state energy are very different to the values obtained by using WGMERT. This difference is not surprising, however, since the parametric form of the photodetachment cross section does not take

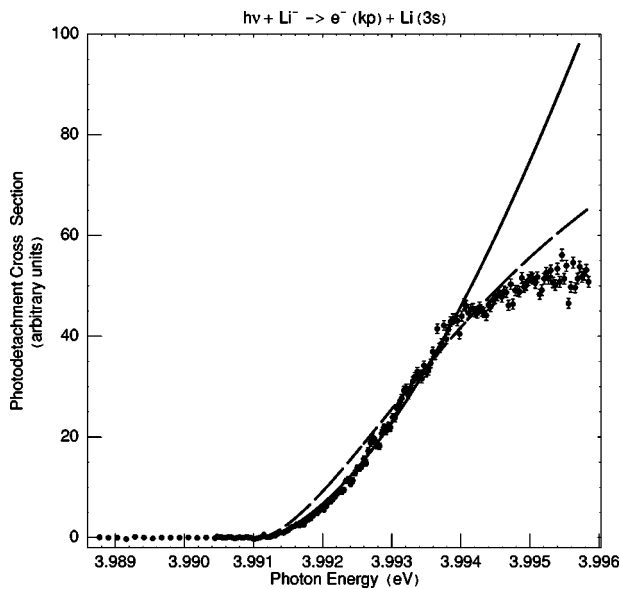


FIG. 5. The relative partial cross section for the photodetachment of  $\text{Li}^-$  into the  $e^-(kp)\text{-Li}(3s)$  continuum above the  $\text{Li}(3s)$  threshold. The experimental data is shown by the black solid circles, the  $p$  wave WG Mert fit by the solid line, and the TOB factor,  $|T|^2$ , normalized to the experimental data, is shown by the dashed line.

into account explicitly the significant polarization potential in the final channel.

Using the  $K_{22}^{P0}(\ell=0)$  value that we extracted from the WG Mert fit to the cross section for photodetachment of  $\text{Li}^-$  via the  $e^-(ks,d)\text{-Li}(2p_{1/2})$  continuum, we deter-

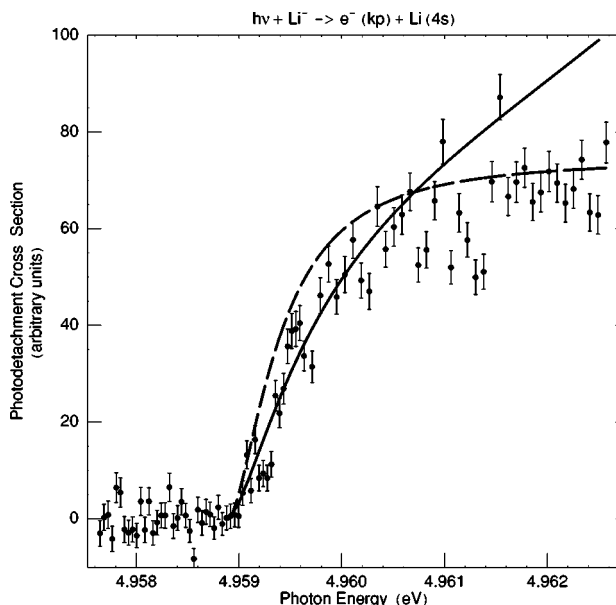


FIG. 6. The relative partial cross section for the photodetachment of  $\text{Li}^-$  into the  $e^-(kp)\text{-Li}(4s)$  continuum above the  $\text{Li}(4s)$  threshold. The experimental data is shown by the black solid circles, the  $p$  wave WG Mert fit by the solid line, and the TOB factor,  $|T|^2$ , normalized to the experimental data, is shown by the dashed line.

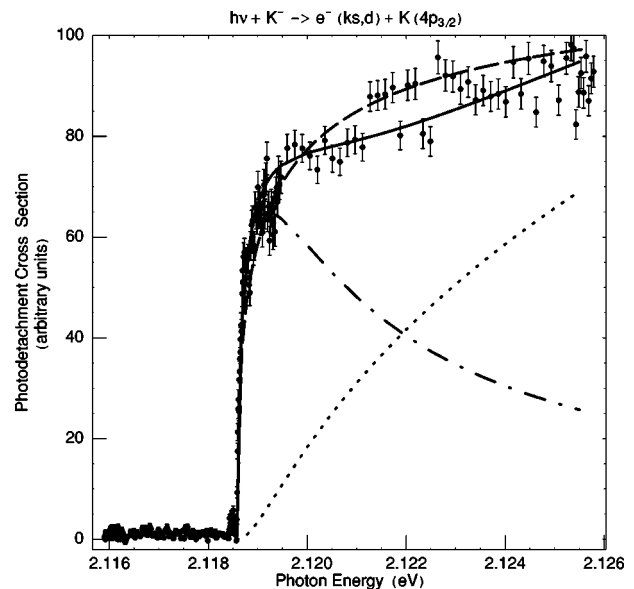


FIG. 7. The relative partial cross section for the photodetachment of  $\text{K}^-$  into the  $e^-(ks,d)\text{-K}(4p_{3/2})$  continuum above the  $\text{K}(4p_{3/2})$  threshold. The experimental data is shown by the black solid circles, the sum of the  $s$  wave and extracted  $d$  wave WG Mert fits by the solid line, the  $s$  wave WG Mert fit by the dashed-dotted line, the extracted  $d$  wave WG Mert fit by the dotted line, and the TOB factor,  $|T|^2$ , normalized to the experimental data, is shown by the dashed line. The very small peak situated just below the threshold is caused by broadband emission from the laser (amplified spontaneous emission).

mined the  $s$  wave phase shift and the elastic cross section for low-energy  $e^-(ks)\text{-Li}(2p_{1/2})$  scattering. Figures 8 and 9 show, respectively, the  $s$  wave phase shift and the elastic cross section.

The behavior of the cross section for photodetachment of  $\text{Li}^-$  into the  $e^-(ks,d)\text{-Li}(3p)$  continuum (see Fig. 4) is similar to that for the photodetachment of  $\text{Li}^-$  into the  $e^-(ks,d)\text{-Li}(2p_{1/2})$  continuum. However, the cross section for the final channel  $e^-(ks,d)\text{-Li}(3p)$  rises much more sharply than the cross section for the final channel  $e^-(ks,d)\text{-Li}(2p_{1/2})$ . The cross section for photodetachment of  $\text{Li}^-$  into the  $e^-(ks,d)\text{-Li}(3p)$  continuum reaches its peak only 0.18 meV above threshold, which corresponds to an energy of approximately 70 times the height of the  $s$  wave barrier. In this case the Wigner law is satisfied over the much smaller energy range of 0.1 meV. This behavior is to be expected

TABLE II. Threshold energies,  $E_{th}$ , in eV obtained by fitting the Wigner law to the near-threshold photodetachment experimental data.

Excited-state atom	$E_{th}$
$\text{Li}(2p_{1/2})$	2.465865(20)
$\text{Li}(3p)$	4.452310(20)
$\text{Li}(3s)$	3.99111(7)
$\text{Li}(4s)$	4.95890(9)
$\text{K}(4p_{3/2})$	2.118573(12)

TABLE III. The low-energy electron scattering quantities and  $K_{22}^{P0}(\ell=0, 1)$  determined from the analysis of the measured  $\text{Li}^-$  and  $\text{K}^-$  near-threshold photodetachment cross sections.

Final state	$K_{22}^{P0}$	$A_0$	$k_p$
$e^-(ks)\text{-Li}(2p)$	$-0.18 \pm 0.02$	$-65 \pm 5$	$-0.0008(1) - i0.01$
$e^-(ks)\text{-Li}(3p)$	$-0.7 \pm 0.3$	$-(2.4 \pm 1.1) \times 10^2$	$-0.0007(3) - i0.002$
$e^-(kp)\text{-Li}(3s)$	$-1.5_{-0.9}^{+0.4}$		$0.02 - i0.02$
$e^-(kp)\text{-Li}(4s)$	$0.8_{-0.3}^{+1.2}$		$0.002(1) - i0.007(1)$
$e^-(ks)\text{-K}(4p_{3/2})$	$-0.08 \pm 0.02$	$-(3.2 \pm 0.7) \times 10^2$	$-0.00005(3) - i0.003(1)$

since the polarizability of  $\text{Li}(3p)$  is approximately 200 times larger than the polarizability of  $\text{Li}(2p)$ . Both the steeper rise in the cross section above threshold and the narrower range of validity of the Wigner law can be attributed to the larger polarizability of  $\text{Li}(3p)$ . The TOB and WGMERT fits reproduce the main shape of both cross sections, namely a sharp rise followed by a plateau region. However, the WGMERT fit for the  $\text{Li}(3p)$  case is not as good as it is for the  $\text{Li}(2p_{1/2})$  case. This can be understood since the  $\text{Li}(3p)$  energy level is very close to the  $\text{Li}(3d)$  level, which accounts for the extremely large polarizability of  $\text{Li}(3p)$ . This also means that the single-channel approximation used in the analysis will not be as good in the case where the final continuum channel is  $e^-(ks, d)\text{-Li}(3p)$ . In the case of photodetachment of  $\text{Li}^-$  via the  $e^-(ks, d)\text{-Li}(3p)$  channel, the TOB factor,  $|T|^2$ , was normalized to the experimental data very close to threshold, at  $E=4.45246$  eV. The  $s$  wave WGMERT cross section was fitted at two points near threshold, at  $E=4.45236$  eV and  $E=4.45249$  eV. The  $d$  wave WGMERT fit to the difference between the experimental data and the  $s$  wave WGMERT cross section was made at two points further away from threshold, at  $E=4.45258$  eV and  $4.45269$  eV. Using the extracted  $K_{22}^{P0}(\ell=0)$ , we determined the value of  $s$  wave scattering length for  $e^-\text{-Li}(3p)$  scattering to be  $-236$ . The position of a virtual-state pole in the single-channel  $S$ -matrix was located to be at  $k_p = -0.0007 - i0.002$  ( $E_{vir} = -0.00006 + i0.00004$  eV). To our knowledge, this is the first prediction of a virtual state in the  $e^-(ks)\text{-Li}(3p)$  system. The  $s$  wave phase shift for  $e^-\text{-Li}(3p)$  elastic scattering rises rapidly from

zero at the  $\text{Li}(3p)$  threshold to a maximum of 0.3 rad at an electron energy  $k^2/2 = 4 \times 10^{-6}$  and then decreases slowly to 0.15 rad at an electron energy of  $k^2/2 = 2 \times 10^{-5}$ . The zero-energy cross section is very large,  $2 \times 10^4 \pi a_0^2$ , due to the presence of the virtual state.

The near-threshold cross section for the photodetachment of  $\text{Li}^-$  into the  $e^-(kp)\text{-Li}(3s)$  continuum (see Fig. 5) rises more slowly with energy than the cross section for the photodetachment of  $\text{Li}^-$  into the  $e^-(ks, d)\text{-Li}(3p)$  continuum. This can be attributed to two factors. First, the photodetachment of  $\text{Li}^-$  into the  $e^-(kp)\text{-Li}(3s)$  continuum, necessitates that the outgoing electron is a pure  $p$  wave. In this case the cross section near threshold, according to the Wigner law, varies as  $k^3$ . Second, the polarizability of the  $\text{Li}(3s)$  state is approximately seven times smaller than the polarizability of the  $\text{Li}(3p)$  state. The experimental cross section for the photodetachment of  $\text{Li}^-$  into the  $e^-(kp)\text{-Li}(3s)$  continuum peaks at an energy approximately 3 meV above threshold. The range of validity of the Wigner law was found to be 1.4 meV in this case. The  $p$  wave WGMERT fit agrees very well with the experimental data near threshold, but starts to deviate from it at 3 meV above threshold, which is the energy at which the experimental cross section begins to flatten. The  $p$  wave WGMERT was fitted to the experimental data at  $E=3.99250$  eV and  $E=3.99382$  eV. The TOB factor,  $|T|^2$ , was normalized to the experimental data near threshold, at  $E=3.99421$  eV. The TOB fit agrees reasonably well with the experimental data near threshold. Using  $K_{22}^{P0}(\ell=1)$  extracted from the WGMERT fit, we found a pole in the single-channel  $S$ -matrix at  $k_p = 0.02 - i0.02$  ( $E_p = 0.001 - i0.008$  eV). The  $p$

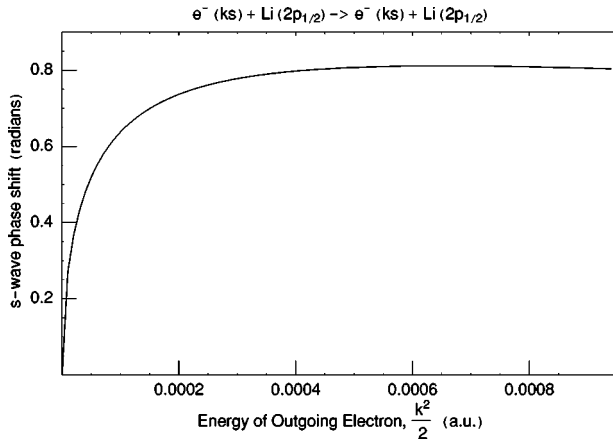


FIG. 8. The  $s$  wave phase shift for elastic  $e^-\text{-Li}(2p_{1/2})$  scattering computed using WGMERT.

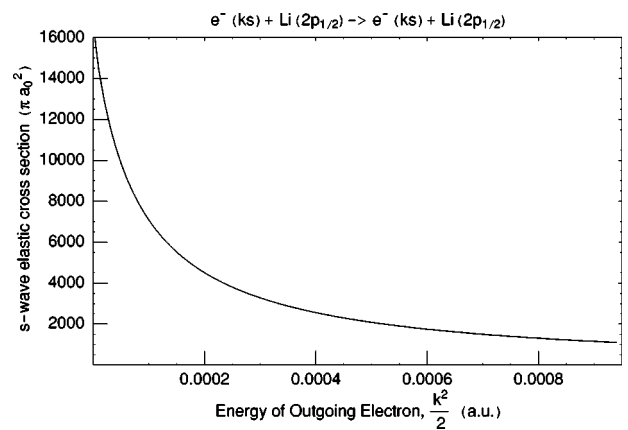


FIG. 9. The elastic cross section for  $e^-\text{-Li}(2p_{1/2})$  scattering computed using WGMERT.

wave phase shift for elastic  $e^-$ -Li(3s) scattering increases monotonically with energy.

The cross section for the photodetachment of  $\text{Li}^-$  into the  $e^-(kp)$ -Li(4s) continuum (Fig. 6) varies more rapidly with energy near threshold than the cross section for the photodetachment of  $\text{Li}^-$  into the  $e^-(kp)$ -Li(3s) continuum. This can be attributed to the fact that the polarizability of Li(4s) state is approximately eight times larger than that of the Li(3s) state. In both processes, the outgoing electron is represented by a pure  $p$  wave. In the case of the  $e^-(kp)$ -Li(4s) process, the range of validity of the Wigner law was determined to be 0.97 meV. The experimental cross section for this channel peaks approximately 1 meV above threshold. The cross section for the photodetachment of  $\text{Li}^-$  into the  $e^-(kp)$ -Li(4s) continuum varies more slowly with energy than that for the photodetachment of  $\text{Li}^-$  into the  $e^-$ -Li(3p) continuum. Again, this can be understood in terms of the Wigner law. According to this law, the threshold energy dependence of the cross section for the photodetachment of  $\text{Li}^-$  into the  $e^-(kp)$ -Li(4s) channel is  $k^3$ , whereas in the case of photodetachment into the  $e^-(ks)$ -Li(3p) channel the energy dependence is  $k$ . Li atoms in the Li(3p) and Li(4s) states have comparable polarizabilities. In the case of the  $e^-(kp)$ -Li(4s) channel, we fitted the  $p$  wave WGMERT cross section to two experimental data points near threshold, at  $E=4.95943$  eV and  $E=4.96003$  eV. The  $p$  wave WGMERT fit to the experimental data is reasonably good for energies up to approximately 3 meV above threshold. We found a pole in the single-channel  $S$ -matrix at  $k_p=0.002-i0.007$  ( $E_p=-0.0006-i0.0004$  eV). This pole corresponds to a resonance with a negative energy position. The parameter  $K_{22}^{P0}(\ell=1)$  for the  $e^-$ -Li(4s) channel is opposite in sign to the same parameter for the  $e^-$ -Li(3s) channel. As a consequence, the  $p$  wave phase shift for  $e^-$ -Li(4s) scattering is remarkably different from the  $p$  wave phase shift for  $e^-$ -Li(3s) scattering. The  $p$  wave phase shift for  $e^-$ -Li(4s) rises from zero at threshold to a maximum of 0.06 rad at an outgoing electron energy of approximately  $2 \times 10^{-5}$  then steadily decreases. The  $p$  wave phase shift passes through zero at an electron energy of approximately  $4 \times 10^{-4}$  which gives rise to a Ramsauer minimum in the corresponding elastic cross section.

The behavior of the cross section for the photodetachment of  $\text{K}^-$  into the  $e^-(ks, d)$ -K(4p<sub>3/2</sub>) continuum (Fig. 7) closely resembles that of the cross section for the photodetachment of  $\text{Li}^-$  into the  $e^-(ks, s)$ -Li(2p<sub>1/2</sub>) continuum. In both cases, the residual atom is left in its first excited state, which is a  $p$  state. The photodetachment cross section of  $\text{K}^-$  has a steeper rise than that of  $\text{Li}^-$ . This is reasonable since the polarizability of K(4p) is approximately five times larger than the polarizability of Li(2p). The photodetachment cross section of  $\text{K}^-$  rises steeply to its peak position at 0.6 meV above threshold, which corresponds to an energy of approximately 40 times the height of the  $p$  wave barrier. The steep rise in the near threshold photodetachment cross section was previously reported by Taylor and Norcross, who performed a four-state close-coupling calculation for the cross section of the photodetachment of  $\text{K}^-$  into the  $e^-(ks)$ -K(4p<sub>3/2</sub>) continuum channel [17]. We found that the  $\text{K}^-$  photodetachment cross sec-

tion satisfies the Wigner law for a limited energy range of 0.2 meV. The  $s$  wave WGMERT gives a good fit to the experimental data very close to threshold. We determined an  $s$  wave scattering length of  $-670$  for  $e^-$ -K(4p<sub>3/2</sub>) scattering. We found a pole in the single-channel  $S$ -matrix at  $k_p=-0.00005-i0.003$  ( $E_{vir}=-0.0001+i0.000004$  eV). This pole corresponds to a virtual state of the  $e^-(ks)$ -K(4p<sub>3/2</sub>) system. From Fig. 7, it can be seen that the  $d$  wave contribution to the photodetachment cross section becomes larger than the  $s$  wave cross section by an energy of only 0.003 eV. This seems unreasonable due to the large centrifugal barrier for the  $d$  wave. Thus, the assumption that the difference between the experimental data and the  $s$  wave WGMERT is purely due to the  $d$  wave contribution is poor. We see that the energy dependence of the parameters  $N'(\ell=0)$  and  $K_{22}^{P0}(\ell=0)$  cannot be neglected. Using  $K_{22}^{P0}(\ell=0)$  we computed the  $s$  wave phase shift for  $e^-$ -K(4p<sub>3/2</sub>) scattering. This phase shift rises from zero at threshold to a maximum of 1.3 rad at an outgoing electron energy of  $5 \times 10^{-5}$ . It then slowly decreases to 0.99 rad at an electron energy of  $2.5 \times 10^{-4}$ . The zero-energy elastic cross section is  $4.4 \times 10^5 \pi a_0^2$ .

## V. CONCLUSIONS

Photodetachment is a process that allows one to gain important information on the structure and dynamics of negative ions. In the present experiment we have investigated, in high resolution, the threshold behavior of photodetachment cross sections involving negative ions of the alkali-metal atoms. Such measurements allow one, in principle, to accurately determine threshold energies and electron affinities. The use of WGMERT to fit the experimental cross section for photodetachment in the threshold region enables the data to be fitted beyond the range of either the Wigner law or the MERT of O'Malley *et al.* Specifically, we have examined the photodetachment of  $\text{Li}^-$  into continuum states in which the excited residual atom was left in both  $p$  states [Li(2p<sub>1/2</sub>) and Li(3p)], and  $s$  states [Li(3s) and Li(4s)]. We have also studied the photodetachment of  $\text{K}^-$  into a continuum state in which the excited residual atom is K(4p<sub>3/2</sub>). This research enabled us to examine the role of the dipole polarization on the threshold behavior. The dipole polarizabilities of the alkali-metal atoms in the five excited states studied are very large. We found that, in all cases, the measured near-threshold cross sections could be fitted to theoretical forms based on the TOB model and the single-channel WGMERT, in which the dipole polarization in the continuum state is taken into account explicitly. Qualitatively, the large polarizabilities of the excited residual atoms were seen to effect dramatically the energy dependence of the near-threshold cross sections. The range of validity of the Wigner law was severely restricted. The cross section for an ejected  $s$  wave electron just above threshold increases rapidly with energy over an extremely narrow energy range and then becomes essentially constant. From the agreement of the WGMERT fits with experimental data, it can be concluded that to describe the near-threshold photodetachment of the alkali-metal negative ion into an excited  $p$  state atom and an outgoing  $s$  wave electron or into an excited  $s$  state atom and an outgoing

$p$  wave electron, it is sufficient to consider only the polarization interaction. Higher order multipole interactions can be neglected. Also, the good agreement of the WGMERT fits with the data indicate that for the channels considered, the single-channel approximation is reasonable. However, it should be noted that we were unable to fit experimental data of the photodetachment of  $\text{Li}^-$  into the  $e^-(ks, d)\text{-Li}(4p)$  continuum channel for the entire energy range with the single-channel version of the WGMERT. This is reasonable since the levels  $4p$ ,  $4d$  and  $4f$  of  $\text{Li}$  are extremely close together. The closeness of the levels accounts for the huge polarizability of  $\text{Li}(4p)$ , namely  $\alpha=236700$  [21].

One of the most interesting outcomes of this work was the ability to extract useful information on low-energy electron scattering on excited targets from the fits to the measured photodetachment thresholds. Direct measurements of electron scattering on excited atoms are very rare due to technical difficulties associated with target preparation. We have determined, for example, the  $s$  wave scattering lengths for  $e^-\text{-Li}(2p_{1/2})$ ,  $e^-\text{-Li}(3p)$  and  $e^-\text{-K}(4p_{3/2})$  scattering. In all cases the scattering lengths were found to be large and negative, indicative of the presence of virtual states, and the corresponding zero-energy elastic cross sections were large.

#### ACKNOWLEDGMENTS

We appreciate discussions with Dr. R. O. Barrachina, Dr. M. Cavagnero, Dr. C. H. Greene, Dr. J. H. Macek, and Dr. H. Sadeghpour. The experimental work was supported by the Swedish Research Council. J.C.H and S.J.W. gratefully acknowledge support from NSF under Grant No. PHY-9780016 and from UNT faculty research grants. S.J.W. gratefully acknowledges support from the Institute for Theoretical Atomic and Molecular Physics at the Harvard-Smithsonian Center for Astrophysics.

#### APPENDIX: THE SINGLE-CHANNEL VERSION OF THE WGMERT FOR THE PARTIAL WAVE PHOTODETACHMENT CROSS SECTION, AND A COMPARISON OF THE VARIOUS MERTS FOR THE PHASE SHIFT $\delta_\ell$

The derivation of the WGMERT and its application to  $\text{K}^-$  photodetachment are given in Ref. [11]. Here, we present briefly the single-channel version that we used to analyze the experimental data.

The partial photodetachment cross section is given by

$$\sigma_{ph}^\ell = N\omega |\langle \Psi_i^- | D | \Psi_0 \rangle|^2 = N\omega |D^z(\ell)|^2, \quad (\text{A1})$$

where  $\ell$  is the orbital angular momentum of the ejected electron,  $N$  is the normalization constant,  $\omega$  is the photon energy and  $D^z(\ell)$  is the dipole matrix element. The kinetic energy of the ejected electron is determined by the energy conservation rule

$$\frac{k^2}{2} = \omega - EA - \Delta, \quad (\text{A2})$$

where  $EA$  is the electron affinity of the atom and  $\Delta$  is the excitation energy of the excited-state residual atom.

In the single-channel approximation the dipole matrix element has the form

$$D^z(\ell) = \left( \frac{k^{\ell+1/2}}{\Gamma_{ff}(\ell) - K_{22}^{P0}(\ell)\Gamma_{gf}(\ell)} \right) D^{P0}(\ell), \quad (\text{A3})$$

where the parameter  $K_{22}^{P0}(\ell)$  varies slowly with energy. The quantity  $D^{P0}(\ell)$  is the part of the dipole matrix element that varies slowly with energy. In Eq. (A3),  $\Gamma_{ff}(\ell)$  and  $\Gamma_{gf}(\ell)$  are elements of the matrix  $\Gamma(\ell)$ . This matrix depends solely on the  $\alpha$ ,  $k$  and  $\ell$ . The elements of the matrix  $\Gamma(\ell)$  vary rapidly with energy and are given by

$$\Gamma_{ff}(\ell) = B_p^{-1/2} k^{\ell+1/2} \cos \xi, \quad (\text{A4})$$

$$\Gamma_{gf}(\ell) = k^{\ell+1/2} (-B_p^{-1/2} \mathcal{G}_p \cos \xi + B_p^{1/2} \sin \xi), \quad (\text{A5})$$

$$\Gamma_{fg}(\ell) = -B_p^{-1/2} k^{-\ell-1/2} \sin \xi, \quad (\text{A6})$$

$$\Gamma_{gg}(\ell) = k^{-\ell-1/2} (B_p^{-1/2} \mathcal{G}_p \sin \xi + B_p^{1/2} \cos \xi), \quad (\text{A7})$$

where, for energies above threshold,  $B_p$ ,  $\mathcal{G}_p$  and  $\xi$  are

$$B_p = (\eta_1^2 + \eta_2^2)^{-1}, \quad (\text{A8})$$

$$\mathcal{G}_p = -B_p(\eta_1\eta_3 + \eta_2\eta_4), \quad (\text{A9})$$

$$\xi = \arctan(\eta_1/\eta_2). \quad (\text{A10})$$

The parameters  $\eta_1$ ,  $\eta_2$ ,  $\eta_3$  and  $\eta_4$  depend only on the characteristic exponent  $\tau$  and the ratio  $m$  of the Mathieu functions, and are given by

$$\eta_1 = \frac{1}{2} \left[ \left( m + \frac{1}{m} \right) + \left( m - \frac{1}{m} \right) \frac{1}{\cos 2\delta} \right], \quad (\text{A11})$$

$$\eta_4 = \frac{1}{2} \left[ \left( m + \frac{1}{m} \right) - \left( m - \frac{1}{m} \right) \frac{1}{\cos 2\delta} \right], \quad (\text{A12})$$

$$\eta_2 = + \frac{1}{2} \left( \frac{1}{m} - m \right) \tan 2\delta, \quad (\text{A13})$$

$$\eta_3 = - \frac{1}{2} \left( \frac{1}{m} - m \right) \tan 2\delta, \quad (\text{A14})$$

where

$$\delta = \frac{\pi}{2} (\tau - \ell - 1/2). \quad (\text{A15})$$

Substituting Eq. (A3) into Eq. (A1) enables the photodetachment cross section to be expressed in terms of the quantities that vary slowly with energy,  $K_{22}^{P0}(\ell)$  and  $D^{P0}(\ell)$ , and quantities that vary rapidly with energy,  $\Gamma_{ff}(\ell)$  and  $\Gamma_{gf}(\ell)$ ,

$$\sigma_{ph}^\ell = \frac{N'(\ell)\omega k^{2\ell+1}}{[\Gamma_{ff}(\ell) - K_{22}^{P0}(\ell)\Gamma_{gf}(\ell)]^2}, \quad (\text{A16})$$

where  $N'(\ell) = N|D^{P0}(\ell)|^2$ . Since  $N'(\ell)$  is defined in terms of  $D^{P0}(\ell)$ , it varies slowly with energy. The WGMERT expres-

sion for the photodetachment cross section, Eq. (A16), correctly satisfies the Wigner law. This can be seen since  $\Gamma_{ff}(\ell)$  tends to  $\pi\alpha^{3/4}k^2/3$  and  $\Gamma_{gf}(\ell)$  tends to  $\alpha^{-1/4}$  as  $k \rightarrow 0$ .

The WGMERT equation for  $\tan \delta_\ell$  for elastic scattering of an electron from a particular excited state of the atom is given by

$$\tan \delta_\ell = k^{2\ell+1} \left( \frac{K_{22}^{P0}(\ell)\Gamma_{gg}(\ell) - \Gamma_{fg}(\ell)}{\Gamma_{ff}(\ell) - K_{22}^{P0}(\ell)\Gamma_{gf}(\ell)} \right). \quad (\text{A17})$$

The WGMERT equation for  $\tan \delta_\ell$  [Eq. (A17)] is equivalent to the MERT developed by O'Malley *et al.* [9] which is given by Eq. (4.3) of their paper. The slowly varying parameter  $B$  in Eq. (4.3) is equal to the negative of  $K_{22}^{P0}(\ell)$  in WGMERT, Eq. (A17). Starting from Eq. (4.3) [9], O'Malley *et al.* considered  $B$  to be linearly dependent on energy and expanded both  $\tau$  and  $m$  in terms of  $fk$ , where  $f = \sqrt{\alpha}$ . This gave rise to the following expressions for  $k \cot \delta_0$  with  $\ell = 0$ ,

$$k \cot \delta_0 = -\frac{1}{A_0} + \frac{\pi\alpha}{3A_0^2}k + \frac{4\alpha}{3A_0}k^2 \ln(0.25\sqrt{\alpha}k) + \dots \quad (\text{A18})$$

and for  $\tan \delta_\ell$  with  $\ell \geq 1$ ,

$$\tan \delta_\ell = \frac{\pi\alpha k^2}{(2\ell-1)(2\ell+1)(2\ell+3)}. \quad (\text{A19})$$

In Eq. (A18),  $A_0$  is the  $s$  wave scattering length which is defined as  $A_0 \equiv -\lim_{k \rightarrow 0} \tan \delta_0/k$ . The  $s$  wave scattering length can be expressed in terms of the slowly varying pa-

rameter  $K_{22}^{P0}(\ell=0)$  according to  $A_0 = \sqrt{\alpha}/K_{22}^{P0}(\ell=0)$  [14]. Equations (A18) and (A19) are the familiar MERT of O'Malley *et al.* [9]. Since an expansion of  $\tau$  and  $m$  in terms of  $fk$  was made in deriving these equations, they are valid only for a very narrow energy range when  $\alpha$  is large.

In FMERT, single-channel scattering is considered and the polarization potential is explicitly taken into account [13]. The FMERT equation for  $\tan \delta_\ell$  is

$$\tan \delta_\ell = -\frac{Mc+d}{Ma+b}, \quad (\text{A20})$$

where  $M$  is a slowly-varying parameter. The coefficients  $a$ ,  $b$ ,  $c$  and  $d$  in Eq. (A20) vary rapidly with energy and depend on  $\alpha$ ,  $k$  and  $\ell$ . The analytical expressions for these coefficients in terms of  $\ell$ ,  $\tau$  and  $m$  are [25]

$$a = -d = \left( \frac{1}{m} - m \right) \cos \pi\tau, \quad (\text{A21})$$

$$b = \left( \frac{1}{m} + m \right) \sin \pi\tau + (-1)^\ell \left( \frac{1}{m} - m \right), \quad (\text{A22})$$

$$c = \left( \frac{1}{m} + m \right) \sin \pi\tau - (-1)^\ell \left( \frac{1}{m} - m \right). \quad (\text{A23})$$

The WGMERT equation for  $\tan \delta_\ell$ , Eq. (A17) is equivalent to the FMERT for  $\tan \delta_\ell$ , Eq. (A20). The slowly-varying parameter  $M$  in the FMERT is equal to the inverse of the slowly-varying parameter  $K_{22}^{P0}$  in the single-channel version of WGMERT. Fabrikant [13] considered  $M$  to depend either linearly with energy or inverse linearly with energy.

- 
- [1] E. P. Wigner, Phys. Rev. **73**, 1002 (1948).  
[2] W. C. Lineberger and B. W. Woodward, Phys. Rev. Lett. **25**, 424 (1970).  
[3] H. Hotop, T. A. Patterson, and W. C. Lineberger, Phys. Rev. A **8**, 762 (1973).  
[4] H. Hotop and W. C. Lineberger, J. Chem. Phys. **58**, 2379 (1973).  
[5] J. Slater, R. H. Read, S. E. Novick, and W. E. Lineberger, Phys. Rev. A **17**, 201 (1978).  
[6] P. Frey, F. Beyer, and H. Holop, J. Phys. B **11**, L589 (1978).  
[7] P. Frey, M. Lawen, F. Breyer, H. Klar, and H. Hotop, Z. Phys. A **304**, 155 (1982).  
[8] N. Rouze and R. Geballe, Phys. Rev. A **27**, 3071 (1983).  
[9] T. F. O'Malley, L. Spruch, and L. Rosenberg, J. Math. Phys. **2**, 491 (1961).  
[10] E. Vogt and G. H. Wannier, Phys. Rev. **95**, 1190 (1954).  
[11] S. Watanabe and C. H. Greene, Phys. Rev. A **22**, 158 (1980).  
[12] M. J. Cavagnero, Phys. Rev. A **50**, 2841 (1994).  
[13] I. I. Fabrikant, Opt. Spectrosc. **53**, 223 (1982) [Opt. Spectrosc. **53**, 131 (1982)].  
[14] S. J. Ward and J. H. Macek, Phys. Rev. A **62**, 052715 (2000).  
[15] S. J. Ward, J. C. Hunnell, and J. H. Macek, Nucl. Instrum. Methods Phys. Res. B **192**, 54 (2002).  
[16] D. L. Moores and D. W. Norcross, Phys. Rev. A **10**, 1646 (1974).  
[17] K. T. Taylor and D. W. Norcross, Phys. Rev. A **34**, 3878 (1986).  
[18] G. Haefliger, D. Hanstorp, I. Kiyon, A. E. Klinkmüller, U. Ljungblad, and D. J. Pegg, Phys. Rev. A **53**, 4127 (1996).  
[19] K. T. Andersson, J. Sandström, I. Yu. Kiyon, D. Hanstorp, and D. J. Pegg, Phys. Rev. A **62**, 022503 (2000).  
[20] C. H. Greene, Phys. Rev. A **42**, 1405 (1990).  
[21] H. Sadeghpour (private communication).  
[22] Y. K. Bae and J. R. Peterson, Phys. Rev. A **32**, 1917 (1985).  
[23] R. K. Nesbet, J. Phys. B **13**, L193 (1980).  
[24] R. O. Barrachina, Nucl. Instrum. Methods Phys. Res. B **124**, 198 (1997).  
[25] D. B. Khrebtukov, J. Phys. A **26**, 6357 (1993).